Graphical Abstract

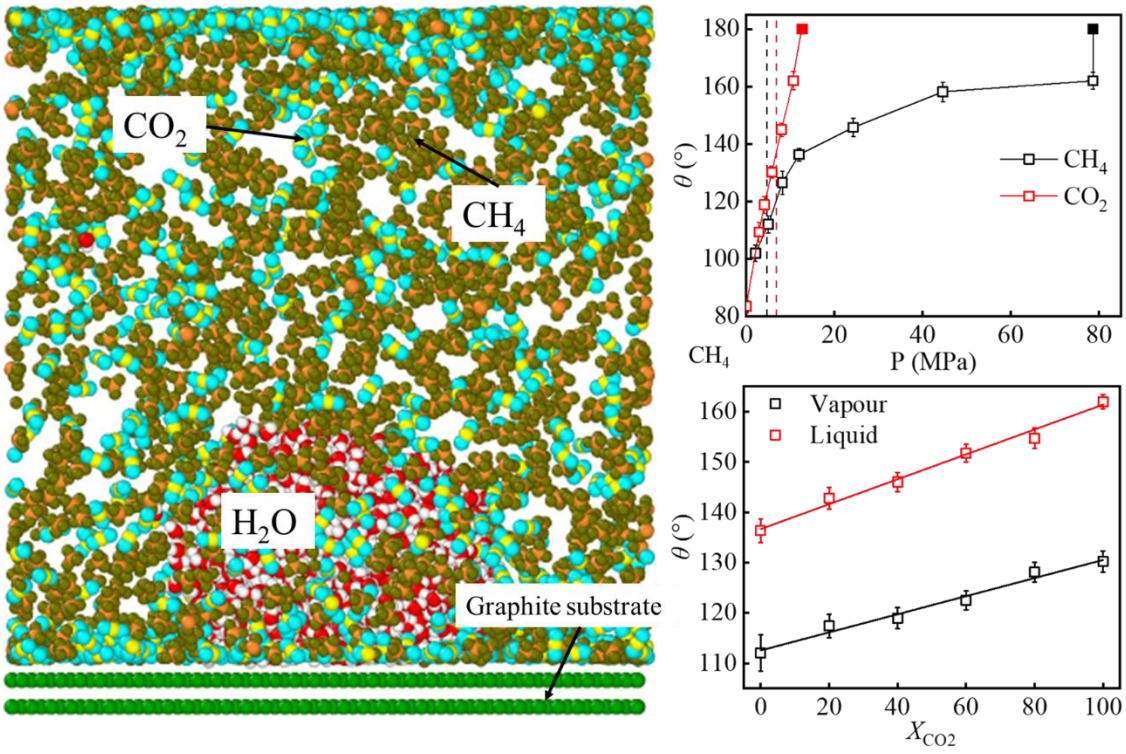

Highlights:

- The microscopic equilibrium contact angle of a water droplet on graphite and immersed in CH_4 or CO_2 is a pronounced function of the absolute pressure.
- Line tension does exhibit a decrease with increasing contact angle.
- A water droplet in organic-rich nanopores immersed in a CH_4 / CO_2 mixture has a contact angle that increases linearly with the CO_2 mole fraction.
- CO_2 exhibits a stronger interaction with organic-rich surface and thus could replace the methane adsorbed on the organic rich solid walls.

The influence of CO_2 and CH_4 mixture on water wettability in organic rich shale nanopore

Wei Yong, Jos Derksen, Yingfang Zhou

School of Engineering, University of Aberdeen, Aberdeen, UK

Abstract

CO_2 has been considered as an effective fluid to replace CH_4 in shale rock. Wetting behavior of water in CO_2 / CH_4 mixtures in organic nanopores is a key parameter influencing CO_2 based enhanced gas recovery processes in shale. However, there is lack of fundamental understanding of water wetting in such systems. We perform Molecular Dynamics (MD) simulations of nanoscopic liquid water drops on a graphite substrate mimicking an organic-rich shale pore in the presence of CH_4/CO_2 mixtures at temperatures in the range 300 K to 400 K. The equilibrium contact angle of the water droplets on graphite is a pronounced function of CH_4 as well as CO_2 pressure with the water droplet lifting-off, that is reaching a 180^o contact angle, at a threshold pressure of 12 MPa for CO_2 and 78 MPa for CH_4. The contact angles recovered from simulations match well with experimental literature via the modified Young's equation. The line tension in our studied systems does not show a specific dependence on temperature. As compared to methane, CO_2 exhibits a stronger interaction with organic-rich surfaces, which has strong impact on wettability. For CH_4/CO_2 mixtures, this translates in an approximately linear increase of the contact angle with the CO_2 mole fraction.

Keywords: Contact angle, Line tension, Water-methane-carbon dioxide, Shale nanopore, Molecular dynamics

1. Introduction

As an alternative to other conventional geo-energy resources, such as coal and oil, shale gas (primary CH_4) has attracted increasing attention due to its lower CO_2 emission after burning (Vedachalam et al., 2015). Shale gas usually exists in the fine-grained sedimentary reservoirs with a very low permeability. The improved hydraulic fracturing and horizonal well technologies have made it possible to produce gas economically from tight shale reservoirs (He et al., 2019; Iddphonce et al., 2020). Capturing carbon dioxide and using it to replace hydrocarbons in geological formations therefore has become a route for mitigating the problem of atmospheric CO_2 and – at the same time – enhancing gas recovery (EGR) from shale (Fathi et al., 2014; Pei et al., 2015; Arif et al., 2017; Louk et al., 2017).

For CO_2 based EGR in shale, water wetting behavior plays a very important role as it determines fluid distribution, spreading and fluid dynamics in the reservoir (Liang et al., 2016; Roshan et al., 2016; Pan et al., 2018; Zhou et al., 2016). The design and operation of CO_2–based EGR benefits from an understanding of the interactions of the various components and associated transport processes at the pore scale. With this in mind, there is an extensive body of experimental literature on multi-component and multi-phase systems in narrow pores. It is beyond the scope of the current paper to review this literature. Experimental methods vary from micro scale to centimeter scale. At the microscale they include microcomputed tomography imaging of pore geometries for the investigation of flooding (Gunde et al., 2010) as well as visualizations of fluids distributions in transparent microfluidic chips (Park, G. et al., 2017). Examples at the centimeter scale are core-flooding experiments probing relative permeability in two-phase porous media flow (Perrin et al., 2009).

From an experimental perspective it is, however, very challenging to realistically replicate the conditions in pores of actual formations, in particular when it comes to tight reservoirs – such as shale – that have pore sizes of the order of tens of nanometers. The nanoscopic length scales make

direct visualization of pore-scale processes virtually impossible, specifically at the high pressures (of the order of up to 80 MPa) representative for reservoir conditions. Artificially increasing pore widths in an experiment to allow for flow visualization is a viable approach that has been reported in (Park, G. et al., 2017). However, physical and chemical processes may not be invariant under scaling up from the nanoscale given the prominence of the molecular nature of matter at this scale.

Additionally, there are properties relevant to wetting that are negligible in macroscopic systems but play a significant role at the molecular level. An example is line tension, which is - by analogy with surface tension - excess free energy associated with unit length of a contact line where three distinct phases coexist (Weijs et al., 2011). The line tension of a three-phase contact line manifests itself at the nanoscale where it has impact on wetting characteristics(Wang, J. Y. et al., 2001), most notable the contact angle. For example around fibers (Bauer and Dietrich, 2000), at liquid (oil lenses/water/air) (Aveyard et al., 1999) and at solid surfaces (Widom, 1995).

Although the line tension is well-defined in thermodynamics long time ago (Gibbs, 1948), line tension studies have often proven controversial over its magnitude, sign, and some substantial issues, such as what leads to line tension (Amirfazli and Neumann, 2004; Schimmele et al., 2007). Descriptions of line tension usually involve density functional theory given its origin in intermolecular forces (Weijs et al., 2011).

Experimentally, the most direct way to determine line tension is to measure the contact angle as a function of contact line curvature (i.e. droplet size). Then line tension can be calculated by using the modified Young's equation (Pethica, 1977). There is, however, significant uncertainty in line tension measurements with estimates ranging over many orders of magnitude: from 10^{-11} to 10^{-5} J/m (Bresme and Oettel, 2007). This uncertainty is attributed to difficulties in determining contact angles, for instance as a result of contact angle hysteresis caused by surface inhomogeneities (Drelich, 1996).

Simulation of pore scale processes – if properly verified and validated – is an approach that complements experimentation. Given that the molecular nature of matter clearly manifests itself at length scales we are interested in, Molecular Dynamics (MD) simulations are an appropriate tool. There is an extensive literature on MD simulations of (nano) pore scale processes as well as on interfacial phenomena. Given our interest in surface phenomena and wetting behavior, relevant work has been reported on interfacial tension and phase equilibrium properties (Miguez et al., 2014; Sakamaki et al., 2011; Yang et al., 2017) and fluid-solid interactions (Iglauer et al., 2012; Khan and Singh, 2014; Werder et al., 2003) including the effects of substrate roughness (Park, J. et al., 2011; Yaghoubi and Foroutan, 2018). Derksen (Derksen, 2015) conducted MD simulations on the deformation and mobility of a droplet attached to a solid substrate as the result of a shear flow.

The aim of this paper is to quantify wettability of (connate) water on surfaces consisting of stacks of graphene sheets mimicking organic-rich shale pores in the presence of methane and carbon dioxide; and thus to better understand the mechanism of the CO_2-based EGR in shale gas exploitation. Stacks of graphene sheets have been extensively reported to accurately mimic actual organic rich pores for a wide range of temperature and pressure in MD simulations. Examples includes water contact angle simulation over organic surface (Werder et al., 2003), methane flow transport in organic shale pores (He et al., 2019; Kazemi and Takbiri-Borujeni, 2016), hydrocarbon adsorption onto organic pore surface (Wang, S. et al., 2016). MD simulation results with organic pores represented by stacks of graphene sheets are consistent with other simulation results and available experimental data (Jin and Firoozabadi, 2015; Jin and Firoozabadi, 2016; Li et al., 2013; Pan et al., 2018). We do this by determining the contact angle of nanoscopic water droplets as a function of pressure and composition of the ambient CH_4/CO_2 mixture. The concept of line tension along with the modified Young's equation allows to extrapolate our findings at the nanoscale to macroscopic contact angles that are amenable to experimental validation.

This paper has been fully studied through MD simulations and is organized in the following manner. In the next section we summarize the simulation methodology as well as the force field parameters used in the MD simulations. We then explain how data have been collected and analyzed. In the *Results* section, we study the relationship between the microscopic and macroscopic contact angle of liquid water on graphite in a water vapour, methane and carbon dioxide environment. We then report results on the microscopic contact angle of liquid water in methane and mixed methane / carbon dioxide environments over a range of pressures, compositions and temperatures and we compare our results with the experimental and computational literature. The final section reiterates the main conclusions of our work and suggests future research directions.

2. Molecular dynamics simulation setup

2.1 Governing equations

In classical MD simulations, forces on an atom are derived from interaction potentials with surrounding atoms. The position and velocity of each atom are then determined by numerically solving Newton's equation of motion

$$\mathbf{F_i} = m_i \frac{d\mathbf{v_i}}{dt} \tag{1}$$

where $\mathbf{v_i} = \frac{d\mathbf{r_i}}{dt}$ is the velocity of atom i, $\mathbf{r_i}$ its position and m_i its mass. The force $\mathbf{F_i}$ it feels is the sum of interaction forces due to atoms surrounding atom i. One distinguishes between inter and intramolecular forces. For intermolecular forces (forces between atoms being part of different molecules) only pairwise interactions are considered. Intramolecular forces (forces between atoms in the same molecule) also involve triple and quadruple interactions. Interaction forces are derived from interaction potentials that only depend on the relative position of the atoms taking part in the

interaction. For pairwise interactions the potential U only depends on the distance between the atom pair i and j $r_{ij} = |\mathbf{r_{ij}}| = |\mathbf{r_i} - \mathbf{r_j}|$. The force on atom i due to a pairwise interaction with atom j is

$$\mathbf{f_{ij}} = -\frac{dU(r_{ij})}{dr_{ij}} \frac{\mathbf{r_i} - \mathbf{r_j}}{r_{ij}} \tag{2}$$

For pairwise interactions we have been using the Lennard-Jones (LJ) potential plus the electrostatic ("Coulombic") potential:

$$U(r_{ij}) = 4\varepsilon_{ij}\left[\left(\frac{\sigma_{ij}}{r_{ij}}\right)^{12} - \left(\frac{\sigma_{ij}}{r_{ij}}\right)^{6}\right] + \frac{q^i q^j}{4\pi\varepsilon_0 r_{ij}} \tag{3}$$

with ε_{ij} and σ_{ij} the strength and the length scale of the LJ interaction respectively, q^i and q^j the charges of sites i and j, and ε_0 the dielectric permittivity of the vacuum. Each atom type α has been given its own size σ_α and strength ε_α. The cross interaction LJ parameters between atoms of different type (α and β) are deduced from the Lorentz−Berthelot mixing rules (Hudson and McCoubrey, 1960): $\sigma_{\alpha\beta} = (\sigma_\alpha + \sigma_\beta)/2$ and $\varepsilon_{\alpha\beta} = \sqrt{\varepsilon_\alpha \varepsilon_\beta}$.

2.2 Model systems

Our simulation systems involve water, CO_2, CH_4 and graphite substrates. A typical situation is given in Figure 1 with a droplet of liquid water on graphite immersed in a CO_2 / CH_4 mixture. The graphite substrate is represented by two graphene sheets at a distance of 3.35Å (Saito et al., 2001). Due to the periodic boundary condition applied, this two-layer graphene sheet substrate is acting like a symmetric solid surface at the top of system. Hence, the whole system – consisting of water, methane and carbon dioxide – is closed off at the top.

For the intramolecular interactions we have been using the SPC/E model for water (Wu et al., 2006), the OPLS models for CH_4 (Aimoli et al., 2014), the Cygan model for CO_2 (Cygan et al., 2012) and a force field proposed by (Stuart et al., 2000) for graphene. These force-fields have been extensively used and validated in a wide body of MD studies. Their results – for example phase

thermodynamic properties (Aimoli et al., 2014; Wu et al., 2006), flow transport characteristic (Aimoli et al., 2014) and adsorption behaviour (Suk and Aluru, 2013)– have been reported with reasonable accuracy. All simulations were performed with the open-source molecular dynamic simulation code LAMMPS (Plimpton, 1995). The LJ interaction potential has been consistently truncated at 10 Å. The long-range electrostatic interactions were computed using the particle-particle-particle-mesh (PPPM) method with the transition between particle-particle to particle-mesh at 10 Å and the relative error set to 10^{-5} (Darden et al., 1993). The velocity Verlet algorithm (Swope et al., 1982) has been used to achieve position and velocity updates with a time step of 2 fs. The complete set of parameters used in the simulations in this paper is given in Table 1.

2.3 Data post-processing

For estimating the contact angle of water on a graphite substrate, a water droplet is placed on the substrate and allowed to equilibrate for 1 ns after which it has reached a dynamically steady shape. Over the subsequent 2 ns an axisymmetric average concentration field is determined through a cylindrical binning procedure (De Ruijter et al., 1999). An example of such an average concentration field is shown in Figure 2 (left panel). A circular arc is then fitted through the points of the field that has a water molecule concentration of 0.02 ($1/Å^3$), i.e. half the bulk water density. In this fitting process points closely above the substrate (i.e. below $Z = Z_0 \sim 10$ Å) are discarded given the layering that occurs there (Werder et al., 2003), see Figure 2 (right). The angle between the fitted arc and the line $Z = 3.35$ Å (the topmost layer of graphene sheets) is our estimate of the contact angle θ. In the example of Figure 2, $\theta = 83.6° \pm 1.1°$. The uncertainty in the contact angle – which is a result of the statistical nature of molecular processes – has been estimated by repeating the process above a number of times (10 times in the example in Figure 2). The uncertainty of 1.1° is the standard deviation of the 10 realizations.

The pressure in MD simulations is usually derived from the pressure tensor $p_{\alpha\beta}$ that can be related to velocities and interaction forces according to a virial expression (Iglauer et al., 2012)

$$p_{\alpha\beta}V = \left\langle \sum_{i=1}^{N} m_i \mathrm{v}_{\alpha,i} \mathrm{v}_{\beta,i} + \sum_{i=1}^{N-1} \sum_{j>1}^{N} r_{\alpha,ij} f_{\beta,ij} \right\rangle \quad (4)$$

with V the volume of the simulation domain, N the total number of atoms, $\mathrm{v}_{\alpha,i}$ the velocity component in the α direction of atom i and $r_{\alpha,ij}$ and $f_{\alpha,ij}$ the α component of vectors $\mathbf{r_{ij}}$ and $\mathbf{f_{ij}}$ respectively. The angled brackets represent ensemble averaging. The pressure p is the average of the three diagonal pressure tensor components: $p = \left(p_{xx} + p_{yy} + p_{zz} \right) / 3$.

In order to relate contact angles measured from nanoscopic droplets – as in the current study – to macroscopic contact angles for which experimental data are available we apply the concept of the modified Young's equation (Pethica, 1977; Veselovsky and Pertsev, 1936)

$$\gamma_{SC} = \gamma_{SL} + \gamma_{LC} \cos\theta + \frac{\tau}{r_B} \quad (5)$$

with τ the line tension, r_B the droplet base radius and γ_{SC}, γ_{SL} and γ_{LC} the solid-continuous phase, solid-liquid and liquid-continuous phase surface tension, respectively. We note that if $1/r_B \to 0$, the macroscopic contact angle θ_∞ is recovered according to $\cos\theta_\infty = (\gamma_{SC} - \gamma_{SL}) / \gamma_{LC}$. As a result, Eq. 5 can be written as

$$\cos\theta = \cos\theta_\infty - \frac{\tau}{\gamma_{LC}} \frac{1}{r_B} \quad (6)$$

The latter representation will be used to determine θ_∞ through extrapolation of data for θ as a function of r_B.

3. Results & discussion

Simulations have been conducted in an NVT ensemble, mostly at a temperature of 300 K. The base-case situation consists of two graphene sheets at a distance 3.35 Å and of size 80×80 Å^2. At the centre of this substrate we place a water droplet consisting of 995 molecules in a semi-spherical shape with a radius of approximately 24.2 Å, i.e. significantly smaller than the side lengths of the substrate. Any additional graphene sheets would not make any difference, as the distance between

water molecules and the graphene sheet (more than three sheets) will be larger than the cut-off distance for the LJ potential (10 Å). The size of the – fully periodic – domain in the direction normal to the substrate is 90 Å. In this domain we place CH_4 and/or CO_2 molecules. By varying the number of molecules surrounding the water droplet we vary the pressure. As an example, with the number of CH_4 molecules ranging from 0 to 7390 zero the pressure ranges from around 0.0014 MPa to 80 MPa, where the pressure in the absence of CH_4 is due to water vapour. The force field parameters of all constituents (water, CH_4, CO_2 and carbon in the graphene sheets) are listed in Table 1. While the AIREBO potential (Stuart et al., 2000) is adopted to include the thermal motion of the carbon atoms in graphene.

We compared the PVT behaviour of CH_4, CO_2, and CH_4/CO_2 mixture (Xco_2= 40%) in confined and unconfined systems. For unconfined system, the solid substrate was not included in the simulations and periodic boundary condition was applied to act as an infinite unconfirmed system. Both corresponding confined and unconfined systems have a same phase density and temperature. Our results find the pressure in unconfined systems matches well with that in confined system – with a difference less than 4% – specifically for pure CH_4 and CO_2 systems. A 6.6% pressure difference is noticed in CH_4/CO_2 mixture system. Additionally, we compared simulated pressures to experimental PVT data (Esper et al., 1989)that shows the experimental value would be up to ~9% higher than unconfined pressure and ~16% higher than confined pressure.

We start by investigating the effects of thermal motion of the graphene sheet on the contact angle in a water-only simulation. In the literature thermal motion of a solid substrate is often discarded in MD simulations (Sedghi et al., 2014; Stukan et al., 2010; Supple and Quirke, 2004). We are interested in the strength of this thermal motion and if it impacts the dynamics of a three-phase contact line and thus the contact angle. We then study effects of the size of the water droplet and – by means of the modified Young's equation (Eq. 5) extrapolate – extrapolate to macroscopic contact angles that can be compared to experimental data from the literature. Next, the line tension

– a non-negligible property in microscopic wetting – is investigated in water only, carbon dioxide and methane environments. Finally, the impact of the composition of the CH_4 / CO_2 on the contact angle is investigated.

Figure 3 summarizes the results regarding thermal motion of the graphite substrate. As can be seen from the left panel, its thermal motion – quantified by the root-mean-square of displacement of carbon atoms in the wall-normal direction – is weak. It is of the order of 0.1 Å which is more than one order of magnitude smaller than the size of the carbon atoms constituting the substrate. There is an obvious but only slight dependence on temperature. It is interesting to note the effect of the number of graphene sheets constituting the graphite surface with a significant transition from 2 to 3 sheets, a transition that consists of two phenomena: reduction of RMS displacement and a weakening of the effect of temperature. This is the result of a smaller thermal motion for carbon atoms located in the middle sheet(s) as compared to the outer sheets for substrates with three or more layers. As an example, at 300 K the two-layer substrate shows an RMS displacement of 0.167 Å for both sheets. At the same temperature a three-layer substrate has RMS displacements of 0.131 Å for the outer sheets and 0.122 Å for the middle sheet.

The right panel of Figure 3 shows contact angles for water-only systems as a function of temperature for fixed and thermally excited graphite. Given the error bars there is no significant difference between the two modi of graphite, except perhaps for 350 K that shows a 2° difference. The above observations are in line with MD simulations of Werder at el (Werder et al., 2003) – their work has been done using the parallel molecular dynamics code FASTTUBE – for water droplets on a 2-layer graphite substrate. According to the simulation results obtained, we conclude that the thermal motion of carbon atoms has very limited influence on contact angle and thus from here on graphite is represented by two graphene sheets at a distance of 3.35 Å consisting of fixed carbon atoms.

3.1 Macroscopic contact angle

The water droplets simulated using molecular dynamic simulation in the current study are of nanoscopic size. Given the modified Young's equation (Eq. 5) we thus expect a dependency of the contact angle on the droplet size. To investigate this, the size of the water droplet has been varied in the range of approximately 15 to 40 Å. The smallest droplet consists of 530 molecules; the largest consist of 5000 molecules. In order to avoid interaction of the droplet with itself over the periodic boundaries, the simulations dealing with droplet size effects have an extended domain volume of $120\times120\times120 Å^3$. We consider three sets of situations: the liquid water droplet is surrounded by water vapour; the droplet is surrounded by CH_4 (3249 molecules which amounts to a pressure of 3.0 MPa); the droplet is surrounded by CO_2 (3249 molecules which amounts to a pressure of 3.5 MPa). The temperature has been fixed to 300 K.

The results of all 15 simulations (5 droplet sizes times 3 situations) have been summarized in Figure 4. They confirm the behaviour anticipated by Eq. 6: a decrease of $\cos\theta$ with increasing $1/r_B$. By fitting straight lines to the data and determining the intercept with the vertical axis $\cos\theta_\infty$ has been estimated. This leads to θ_∞ estimates of 78.9 ± 2.9°, 99.6 ± 2.1° and 111.3 ± 2.3° for H_2O-only, H_2O/CH_4, and H_2O/CO_2 respectively. The uncertainty in $\cos\theta_\infty$ is a result of a weighted least squares straight line fitting based on the uncertainties in the individual data points.

The water-only value at T = 300K and 350 K is quantified in Figure 5 and is well in line with experimental data on the water contact angle on chemically pure graphene: 79.3° at room temperature and atmospheric pressure (Li et al., 2013). Siemons et al (Siemons et al., 2006) experimentally studied the pressure dependence of the contact angle in CO_2–water–coal systems. From their work an angle of 117.0^o can be estimated at P=3.5 MPa and T=318 K. Sakurovs et al (Sakurovs and Lavrencic, 2011) measured a 109° contact angle of water on a carbon-rich coal sample (88.4% carbon content) in an environment of CO_2 at P=3.5 MPa and T=313 K. These two

experimental values agree fairly well with our simulated angle of approximately 111.3°. As of yet we have not found experimental data of water on carbon-rich substrates in a methane environment.

3.2 Line tension

As pointed above, given the realistic length scale of pore in shale formation, the line tension of a three-phase contact line plays a important role in wetting behavior during EGR process in shale (Wang, J. Y. et al., 2001). As shown in Equation 6, it allows to determine the line tension τ from the slope of the fitted lines in Figure 4 along with the surface tension between the water droplet and its surroundings. For the water only system we have a surface tension of 72 mN/m (Speight, 2019) for water-air interface at 293K. Then the resulting line tension is $\tau = (1.51 \pm 1.1) \times 10^{-11}$ J/m with the significant uncertainties due to the uncertainties in the data points in Figure 4. This is in line with the results from Mugele et al's atomic microscopic experiments (Mugele et al., 2002) and theoretical predictions using statistical mechanics (Dobbs and Indekeu, 1993; Getta and Dietrich, 1998) that report values in a range of 10^{-12} to 10^{-10} J/m. Mugele et al combined atomic force microscopy data to determine the contact angle of micrometre size droplets and the conventional optical method for millimetre size droplets, all on homogeneous substrates. They were able to estimate an upper limit of line tension as $\tau \sim 10^{-10}$ J/m.

H_2O/CH_4 has a surface tension of γ_{LC} =68.32 mN/m at T= 298.15K and P= 5MPa (Ren et al., 2000); H_2O/CO_2 has γ_{LC} =55.42 mN/m at T= 297.9K and P= 3MPa (Georgiadis et al., 2010). Given the slopes of the fits in Figure 4 we then estimate $\tau = (1.49 \pm 0.64) \times 10^{-11}$ J/m and $\tau = (0.71 \pm 0.5) \times 10^{-11}$ J/m for H_2O/CH_4 and H_2O/CO_2 respectively.

The sensitivity of line tension with respect to temperature has been assessed by performing the same set of simulations but now at 350 K with surface tension data at this temperature also from (Georgiadis et al., 2010; Ren et al., 2000). All line tension data points are presented in Figure 6. Given the relatively large uncertainties we cannot discern a trend with temperature. We can say

with some certainty, however, that the H_2O/CO_2 systems – that are more hydrophobic compared to the other two systems – have a lower line tension. This phenomenon – a decrease of line tension with increasing contact angle – is in line with other authors' MD results for ~~the~~ line tension (Werder et al., 2003; Włoch et al., 2017; Zhang et al., 2018), as shown in figure 7. Wloch et al (Włoch et al., 2017) studied water droplets on graphene and Zhang et al (Zhang et al., 2018) probed the interaction between water and a platinum surface. As already noted above, Werder et al (20) dealt with water on graphene. These authors adjusted the water-solid interaction strength to achieve different levels of hydrophobicity. The line tension is then calculated via the same procedure as in the current study. Uncertainties in line tension values were not reported in (Werder et al., 2003; Włoch et al., 2017; Zhang et al., 2018).

3.3 Contact angle as a function of CH_4-CO_2 mixture composition

We now turn to a systematic study of water on graphene in CH_4, CO_2 as well as in CH_4-CO_2 mixture environments under the base-case conditions (NVT ensemble at 300 K; two graphene sheets at a distance 3.35 Å and of size 80×80 $Å^2$; a water droplet consisting of 995 molecules; a domain size normal to the substrate is 90 Å). The main variables are the pressure and the composition of the mixture.

Figure 8 qualitatively shows wetting behaviour in pure CH_4 and CO_2 environments as a function of pressure. It is clear that at the substrate CH_4 as well as CO_2 molecules tend to displace water molecules leading to de-wetting and eventually – at sufficiently high pressure – detachment of the droplet. This has been quantified in Figure 9. The contact angle of water increases significantly for both background fluids, consistent with experimental literature data (Pan et al., 2018). For CO_2 the contact angle increases approximately linearly with pressure – including the cross-over of CO_2 from vapour to liquid – until the droplet detaches at a pressure of 12 MPa. This phenomenon has also been observed in the experimental work presented in (Pan et al., 2018;

Saghafi et al., 2014). For CH_4 the relationship between pressure and contact angle is clearly non-linear, specifically for pressures beyond the critical pressure (4.6 MPa at 300 K). The trend shows a levelling off of the contact angle with pressure – only a 2.5% increase from around 45 to 78 MPa – until the droplet detaches.

It is noteworthy that in our simulations a water droplet detaches from a graphite surface at sufficiently high pressure in a CH_4 as well as in a CO_2 environment. The fully hydrophobic state in a CO_2 environment has also been found in the literature (Liu et al., 2010; Pan et al., 2018). A sudden detachment happens in a CH_4 environment at a high pressure of approximately 78 MPa. For pressures relevant to storing carbon dioxide, a non-water wetting (high pressure) condition is not favourable to consider safe CO_2 geological storage as it may leads to potential leakage (Naylor et al., 2011), and thus the pressure needs to be assessed carefully when determining CO_2 geological storage site.

As reported in the literature (Iglauer et al., 2012; Xu et al., 2017), CO_2 injection is considered to be as an efficient approach to improve CH_4 recovery in tight formations, such as shale or coal bed methane reservoirs. One of the essential properties in this respect is the wettability as it influences the nano-pore conductivity and fluid configuration (Roshan et al., 2016). We now report on MD simulations to estimate the impact of adding CO_2 to CH_4 on the contact angle of water on a graphite surface. The mole fraction X_{CO_2} has been varied between 0% and 100% at further base-case conditions (most importantly a fixed temperature of 300 K). We consider situations with CO_2 in the vapour state and in the liquid state by simulating a total of 1872 molecules of CO_2 plus CH_4 and 3744 molecules of CO_2 plus CH_4 respectively. The respective pressures are 5.36 ± 0.1 MPa and 10.70 ± 0.2MPa.

Contact angle versus X_{CO_2} is shown in Figure 10. Clearly the contact angle increases with increasing X_{CO_2}, tentatively in a linear fashion. The slopes of the two lines in Figure 10 are 0.180^o

per %CO_2 (vapour) and 0.247° per %CO_2 (liquid). These results show that CO_2 changes the wettability of organic-rich surface to a significant extent dependent on mole fraction, pressure and (possibly) temperature. This change is attributed to the stronger interaction between CO_2 – as compared to CH_4 – with the graphene sheets. This can be appreciated from the concentration profiles in the direction normal to the substrate as presented in Figure 11. The displacement of CH_4 by CO_2 is a well-known phenomenon that – for instance – has been reported in (Klewiah et al., 2020; Merey and Sinayuc, 2016; Perera et al., 2012).

4. Summary & conclusions

In this article, we have presented a systematic study of the interactions between water, methane and carbon dioxide in organic-rich shale nanopores over a range of pressures, compositions and temperatures with MD simulations based on a full-atoms approach. The conclusions of our simulation are:

- Consistent with available data from the literature, we find that line tension is positive and of the order of 10^{-11} J/m. Statistical uncertainties make it not possible to discern a trend of line tension with temperature (in the range 300 – 350 K). Line tension does exhibit a decrease with increasing contact angle, something reported earlier in MD-based studies.
- The microscopic equilibrium contact angle of a water droplet on graphite and immersed in CH_4 or CO_2 is a pronounced function of the absolute pressure. This behavior is mainly attributed to the strong fluids interactions with the organic surface when CO_2 or CH_4 pressure rapidly increased. The droplet lifts off beyond a pressure of 12 MPa and 78 MPa for CO_2 and CH_4, respectively.
- A water droplet in organic-rich nanopores immersed in a CH_4 / CO_2 mixture has a contact angle that increases linearly with the CO_2 mole fraction. The slope of the linear trend line depends on pressure.

- In relation to EGR in shale gas exploitation, CO_2 exhibits a stronger interaction with organic-rich surface and thus could replace the methane adsorbed on the organic rich solid walls to improve the methane production, while simultaneously store CO_2 at subsurface.

In this paper we have been studying water wettability in ideal, atomically smooth shale nanopores. In the future we will be working on wettability on heterogeneous and nano-scale rough surfaces to account for more complicated situations and investigate the methane and methane-water flow transport.

Acknowledgments

W. Yong thanks China Scholarship Council's financial support for his Ph.D. study (No. 201708060349).

References

Aimoli, C.G., Maginn, E.J., Abreu, C.R., 2014. Transport properties of carbon dioxide and methane from molecular dynamics simulations. The Journal of chemical physics. 141, 134101.

Amirfazli, A., Neumann, A.W., 2004. Status of the three-phase line tension: a review. Advances in colloid and interface science. 110, 121-141.

Arif, M., Lebedev, M., Barifcani, A., Iglauer, S., 2017. Influence of shale- total organic content on CO2 geo- storage potential. Geophysical research letters. 44, 8769-8775.

Aveyard, R., Clint, J.H., Nees, D., Paunov, V., 1999. Size-dependent lens angles for small oil lenses on water. Colloids and Surfaces A: Physicochemical and Engineering Aspects. 146, 95-111.

Bauer, C., Dietrich, S., 2000. Shapes, contact angles, and line tensions of droplets on cylinders. Physical Review E. 62, 2428.

Bresme, F., Oettel, M., 2007. Nanoparticles at fluid interfaces. Journal of Physics: Condensed Matter. 19, 413101.

Curtis, J.B., 2002. Fractured shale-gas systems. AAPG bulletin. 86, 1921-1938.

Cygan, R.T., Romanov, V.N., Myshakin, E.M., 2012. Molecular simulation of carbon dioxide capture by montmorillonite using an accurate and flexible force field. The Journal of Physical Chemistry C. 116, 13079-13091.

Darden, T., York, D., Pedersen, L., 1993. Particle mesh Ewald: An N· log (N) method for Ewald sums in large systems. The Journal of chemical physics. 98, 10089-10092.

De Ruijter, M.J., Blake, T.D., De Coninck, J., 1999. Dynamic wetting studied by molecular modeling simulations of droplet spreading. Langmuir. 15, 7836-7847.

Derksen, J.J., 2015. Droplets sliding over shearing surfaces studied by molecular dynamics. AIChE Journal. 61, 4020-4027.

Dobbs, H.T., Indekeu, J.O., 1993. Line tension at wetting: interface displacement model beyond the gradient-squared approximation. Physica A: Statistical Mechanics and its Applications. 201, 457-481.

Drelich, J., 1996. The significance and magnitude of the line tension in three-phase (solid-liquid-fluid) systems. Colloids and Surfaces-A-Physiochemical and Engineering Aspects. 116, 43-54.

Esper GJ, Bailey DM, Holste JC, Hall KR., 1989. Volumetric behavior of near-equimolar mixtures for CO2+ CH4 and CO2+ N2. Fluid Phase Equilibria. 49, 35-47.

Fathi, E.; Akkutlu, I. Y., 2014. Multi-component gas transport and adsorption effects during CO2 injection and enhanced shale gas recovery. International Journal of Coal Geology. 123, 52−61.

Georgiadis, A., Maitland, G., Trusler, J.M., Bismarck, A., 2010. Interfacial tension measurements of the (H2O CO2) system at elevated pressures and temperatures. Journal of Chemical & Engineering Data. 55, 4168-4175.

Getta, T., Dietrich, S., 1998. Line tension between fluid phases and a substrate. Physical Review E. 57, 655-671.

Gibbs, J.W., 1948. The collected works of J. Willard Gibbs. Yale Univ. Press, New Haven.

Gunde, A.C., Bera, B., Mitra, S.K., 2010. Investigation of water and CO2 (carbon dioxide) flooding using micro-CT (micro-computed tomography) images of Berea sandstone core using finite element simulations. Energy. 35, 5209-5216.

He, J., Ju, Y., Kulasinski, K., Zheng, L., Lammers, L., 2019. Molecular dynamics simulation of methane transport in confined organic nanopores with high relative roughness. Journal of Natural Gas Science and Engineering. 62, 202-213.

Hudson, G.H., McCoubrey, J.C., 1960. Intermolecular forces between unlike molecules. A more complete form of the combining rules. Transactions of the Faraday Society. 56, 761-766.

Iddphonce, R., Wang, J. and Zhao, L., 2020. Review of CO2 injection techniques for enhanced shale gas recovery: Prospect and challenges. Journal of Natural Gas Science and Engineering Volume 77, May 2020, 103240.

Iglauer, S., Mathew, M.S., Bresme, F., 2012. Molecular dynamics computations of brine–CO2 interfacial tensions and brine–CO2–quartz contact angles and their effects on structural and residual trapping mechanisms in carbon geo-sequestration. Journal of colloid and interface science. 386, 405-414.

Jin, Z., Firoozabadi, A., 2015. Flow of methane in shale nanopores at low and high pressure by molecular dynamics simulations. The Journal of chemical physics. 143, 104315.

Jin, Z., Firoozabadi, A., 2016. Phase behavior and flow in shale nanopores from molecular simulations. Fluid Phase Equilibria. 430, 156-168.

Kazemi, M., Takbiri-Borujeni, A., 2016. Flow of Gases in Organic Nanoscale Channels: A Boundary-Driven Molecular Simulation Study. Energy & Fuels. 30, 8156-8163.

Khan, S., Singh, J.K., 2014. Wetting transition of nanodroplets of water on textured surfaces: a molecular dynamics study. Molecular Simulation. 40, 458-468.

Klewiah, I., Berawala, D.S., Alexander Walker, H.C., Andersen, P.Ø, Nadeau, P.H., 2020. Review of experimental sorption studies of CO2 and CH4 in shales. Journal of Natural Gas Science and Engineering. 73, 103045.

Li, Z., Wang, Y., Kozbial, A., Shenoy, G., Zhou, F., McGinley, R., Ireland, P., Morganstein, B., Kunkel, A., Surwade, S.P., 2013. Effect of airborne contaminants on the wettability of supported graphene and graphite. Nature materials. 12, 925.

Liang, L. X.; Luo, D. X.; Liu, X. J.; Xiong, J. Experimental study on the wettability and adsorption characteristics of Longmaxi Formation shale in the Sichuan Basin, China. Journal of Natural Gas Science and Engineering. 2016, 33, 1107−111.

Liu, S., Yang, X., Qin, Y., 2010. Molecular dynamics simulation of wetting behavior at CO 2/water/solid interfaces. Chinese Science Bulletin. 55, 2252-2257.

Louk, K., Ripepi, N., Luxbacher, K., Gilliland, E., Tang, X., Keles, C., Schlosser, C., Diminick, E., Keim, S., Amante, J. and Michael, K., 2017. Monitoring CO2 storage and enhanced gas recovery in unconventional shale reservoirs: Results from the Morgan County, Tennessee injection test. Journal of Natural Gas Science and Engineering 45: 11-25.

Merey, S., Sinayuc, C., 2016. Analysis of carbon dioxide sequestration in shale gas reservoirs by using experimental adsorption data and adsorption models. Journal of Natural Gas Science and Engineering. 36, 1087-1105.

Miguez, J.M., Garrido, J.M., Blas, F.J., Segura, H., Mejía, A., Piñeiro, M.M., 2014. Comprehensive characterization of interfacial behavior for the mixture CO2 H2O CH4: Comparison between atomistic and coarse grained molecular simulation models and density gradient theory. The Journal of Physical Chemistry C. 118, 24504-24519.

Mugele, F., Becker, T., Nikopoulos, R., Kohonen, M., Herminghaus, S., 2002. Capillarity at the nanoscale: an AFM view. Journal of adhesion science and technology. 16, 951-964.

Naylor, M., Wilkinson, M., Haszeldine, R.S., 2011. Calculation of CO2 column heights in depleted gas fields from known pre-production gas column heights. Marine and Petroleum Geology. 28, 1083-1093.

Pan, B., Li, Y., Wang, H., Jones, F., Iglauer, S., 2018. CO2 and CH4 wettabilities of organic-rich shale. Energy Fuels. 32, 1914-1922.

Park, G., Kim, S., Lee, M., Wang, S., 2017. Microfluidic study for investigating migration and residual phenomena of supercritical CO2 in porous media. Energy Procedia. 125, 520-526.

Park, J., Ha, M., Choi, H., Hong, S., Yoon, H., 2011. A study on the contact angles of a water droplet on smooth and rough solid surfaces. Journal of Mechanical Science and Technology. 25, 323.

Pei, P., Ling, K., He, J., Liu, Z., 2015. Shale gas reservoir treatment by a CO2-based technology. Journal of Natural Gas Science and Engineering. 26, 1595-1606.

Perera, M.S.A., Ranjith, P.G., Viete, D.R., Choi, S.K., 2012. The effects of injection and production well arrangement on carbon dioxide sequestration in deep, unmineable coal seams: A numerical study. International Journal of Coal Preparation and Utilization. 32, 211-224.

Perrin, J., Krause, M., Kuo, C., Miljkovic, L., Charoba, E., Benson, S.M., 2009. Core-scale experimental study of relative permeability properties of CO2 and brine in reservoir rocks. Energy Procedia. 1, 3515-3522.

Pethica, B.A., 1977. The contact angle equilibrium. Journal of colloid and interface science. 567-569.

Plimpton, S., 1995. Fast parallel algorithms for short-range molecular dynamics. Journal of computational physics. 117, 1-19.

Ren, Q., Chen, G., Yan, W., Guo, T., 2000. Interfacial tension of (CO2 CH4) water from 298 K to 373 K and pressures up to 30 MPa. Journal of Chemical & Engineering Data. 45, 610-612.

Roshan, H., Al-Yaseri, A.Z., Sarmadivaleh, M., Iglauer, S., 2016. On wettability of shale rocks. Journal of colloid and interface science. 475, 104-111.

Saghafi, A., Pinetown, K., Javanmard, H., 2014. Gas wettability of coal and implications for gas desorption and drainage. Geofluids. 14, 310-325.

Saito, R., Matsuo, R., Kimura, T., Dresselhaus, G., Dresselhaus, M.S., 2001. Anomalous potential barrier of double-wall carbon nanotube. Chemical physics letters. 348, 187-193.

Sakamaki, R., Sum, A.K., Narumi, T., Ohmura, R., Yasuoka, K., 2011. Thermodynamic properties of methane/water interface predicted by molecular dynamics simulations. The Journal of chemical physics. 134, 144702.

Sakurovs, R., Lavrencic, S., 2011. Contact angles in CO2-water-coal systems at elevated pressures. International Journal of Coal Geology. 87, 26-32.

Schimmele, L., Napiórkowski, M., Dietrich, S., 2007. Conceptual aspects of line tensions. The Journal of chemical physics. 127, 164715.

Sedghi, M., Piri, M., Goual, L., 2014. Molecular dynamics of wetting layer formation and forced water invasion in angular nanopores with mixed wettability. The Journal of chemical physics. 141, 194703.

Siemons, N., Bruining, H., Castelijns, H., Wolf, K., 2006. Pressure dependence of the contact angle in a CO2–H2O–coal system. Journal of colloid and interface science. 297, 755-761.

Speight, J.G., 2019. Natural Water Remediation: Chemistry and Technology, Thermodynamics of water. Butterworth-Heinemann, Oxford.

Stuart, S.J., Tutein, A.B., Harrison, J.A., 2000. A reactive potential for hydrocarbons with intermolecular interactions. The Journal of chemical physics. 112, 6472-6486.

Stukan, M.R., Ligneul, P., Crawshaw, J.P., Boek, E.S., 2010. Spontaneous imbibition in nanopores of different roughness and wettability. Langmuir. 26, 13342-13352.

Suk, M.E., Aluru, N.R., 2013. Molecular and continuum hydrodynamics in graphene nanopores. RSC advances. 3, 9365-9372.

Supple, S., Quirke, N., 2004. Molecular dynamics of transient oil flows in nanopores I: Imbibition speeds for single wall carbon nanotubes. The Journal of chemical physics. 121, 8571-8579.

Swope, W.C., Andersen, H.C., Berens, P.H., Wilson, K.R., 1982. A computer simulation method for the calculation of equilibrium constants for the formation of physical clusters of molecules: Application to small water clusters. The Journal of chemical physics. 76, 637-649.

Vedachalam, N., Srinivasalu, S., Rajendran, G., Ramadass, G.A., Atmanand, M.A., 2015. Review of unconventional hydrocarbon resources in major energy consuming countries and efforts in realizing natural gas hydrates as a future source of energy. Journal of Natural Gas Science and Engineering. 26, 163-175.

Veselovsky, V.S., Pertsev, V.N., 1936. Adhesion of the bubbles to solid surfaces. J.Phys.Chem.(USSR). 8, 245-259.

Wang, J.Y., Betelu, S., Law, B.M., 2001. Line tension approaching a first-order wetting transition: Experimental results from contact angle measurements. Physical Review E. 63, 031601.

Weijs, J.H., Marchand, A., Andreotti, B., Lohse, D., Snoeijer, J.H., 2011. Origin of line tension for a Lennard-Jones nanodroplet. Physics of fluids. 23, 022001.

Werder, T., Walther, J.H., Jaffe, R.L., Halicioglu, T., Koumoutsakos, P., 2003. On the water−carbon interaction for use in molecular dynamics simulations of graphite and carbon nanotubes. The Journal of Physical Chemistry B. 107, 1345-1352.

Widom, B., 1995. Line tension and the shape of a sessile drop. J. Phys. Chem. 99, 2803-2806.

Włoch, J., Terzyk, A.P., Kowalczyk, P., 2017. New forcefield for water nanodroplet on a graphene surface. The Journal of Physical Chemistry. 674, 98-102.

Wu, Y., Tepper, H.L., Voth, G.A., 2006. Flexible simple point-charge water model with improved liquid-state properties. The Journal of chemical physics. 124, 024503.

Xu, R., Zeng, K., Zhang, C., Jiang, P., 2017. Assessing the feasibility and CO2 storage capacity of CO2 enhanced shale gas recovery using Triple-Porosity reservoir model. Applied Thermal Engineering. 115, 1306-1314.

Yaghoubi, H., Foroutan, M., 2018. Molecular investigation of the wettability of rough surfaces using molecular dynamics simulation. Physical Chemistry Chemical Physics. 20, 22308-22319.

Yang, Y., Narayanan Nair, A.K., Sun, S., 2017. Molecular dynamics simulation study of carbon dioxide, methane, and their mixture in the presence of brine. The Journal of Physical Chemistry B. 121, 9688-9698.

Zhang, J., Wang, P., Borg, M.K., Reese, J.M., Wen, D., 2018. A critical assessment of the line tension determined by the modified Young's equation. Physics of Fluids. 30, 82003.

Zhou, Y., Hatzignatiou, D.G. and Helland, J.O., 2016. Computation of three-phase capillary pressure curves and fluid configurations at mixed-wet conditions in 2D rock images. SPE Journal 21 (01), 152-169.

Figure

Table1. Interaction potential functions and their parameters for the chemical species considered.

un-bonded	atom type	mass g/mol	σ & r_{co} Å	ε kcal/mol	q e
$U_{LJ} = 4\varepsilon\left(\frac{\sigma^{12}}{r^{12}} - \frac{\sigma^{6}}{r^{6}}\right)$	C graphite [a]	12.01	3.400 10	0.0684	0.000
	C CH_4 [b]	12.01	3.500 10	0.0660	–0.240
	H CH_4 [b]	1.008	2.500 10	0.0300	0.060
	C CO_2 [c]	12.01	2.800 10	0.0559	0.6512
$U_C = \frac{e^2}{\varepsilon_0}\frac{q_i q_j}{r_{ij}}$	O CO_2 [c]	16.00	3.028 10	0.1597	–0.3256
	O H_2O [d]	15.99	3.166 10	0.1560	-0.8476
	H H_2O [d]	1.008	0.000 10	0.0000	0.4238
bonds	bond type	k kcal/mol·Å^2	r_0 Å		
$U_b = k\ (r_{ij} - r_0)^2$	C–H CH_4	340	1.09		
	C=O CO_2	1008.24	1.16		
	H–O H_2O	∞	1.00		
angles	angle type	k_a kcal/mol·rad^2	θ_0 rad		
$U_a = k_a\ (\theta_{ijk} - \theta_0)^2$	H–C–H CH_4	33.0	1.88		
	O=C=O CO_2	53.965	π		
	H–O–H H_2O	∞	1.91		

[a][Graphite] [31]; [b] [OPLS methane] [29]; [c] [Cygan CO_2] [30]; [d] [SPC/E H_2O] [28];

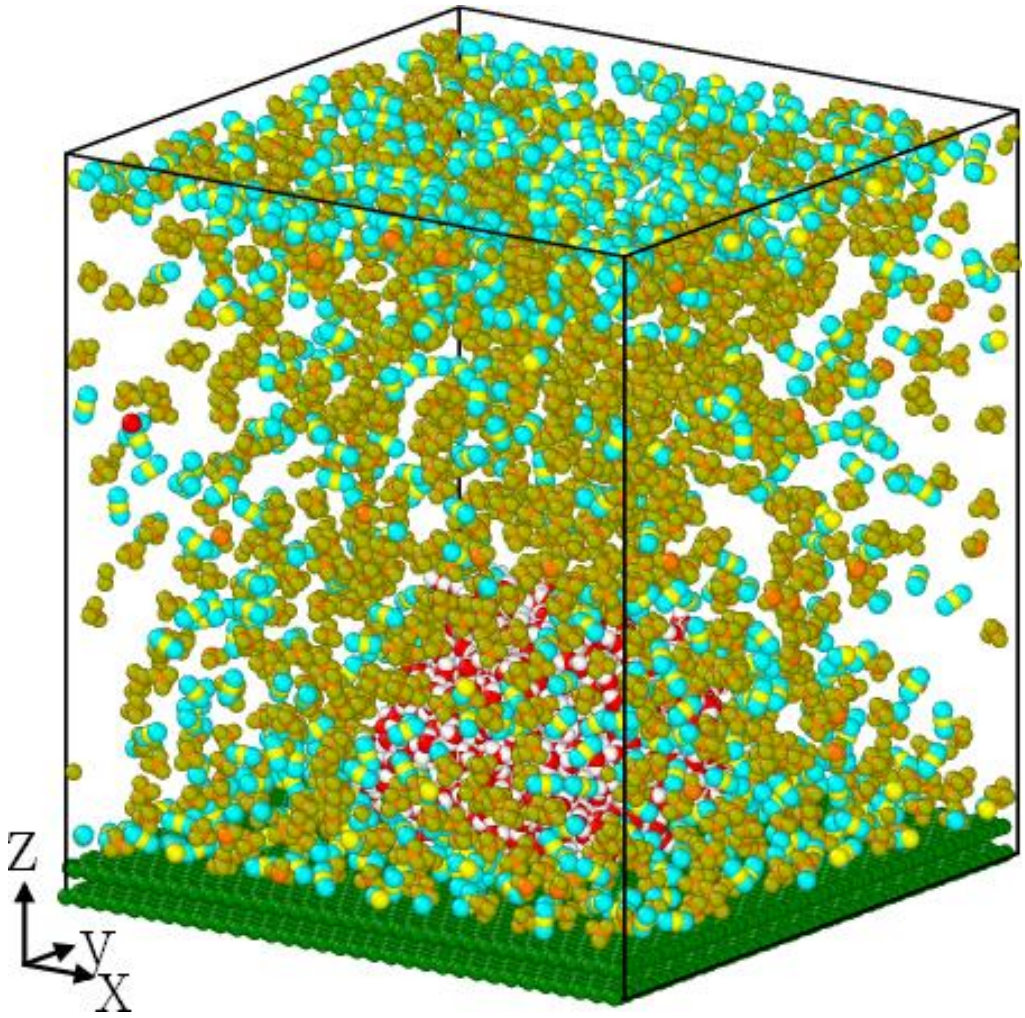

Figure 1. A three-dimensional view of the configuration of a Water-CH_4-CO_2-Carbon system at T=300K and P=5.36 MPa. Green is graphite surface, Yellow and blue are C and O in CO2, Orange and olive are C and H in methane, Red and white represent O and H in water.

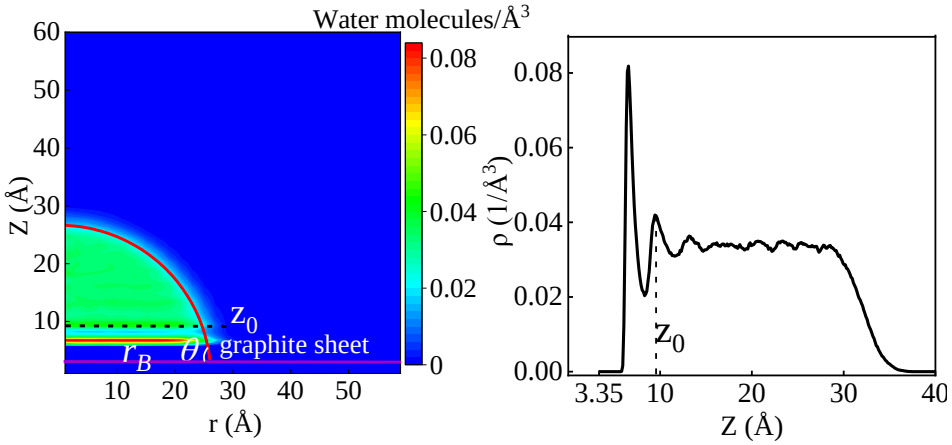

Figure 2. Left: an example of extracting the contact angle θ from an average axisymmetric water concentration field. The red curve is a circular arc fitted through points with concentration 0.02 (1/Å^3) and Z > Z_0 ~10Å to exclude the near wall region. The purple line denotes to top surface of the graphite substrate. The droplet has a base radius r_B. Right: vertical time-average concentration profile along the centreline of the droplet.

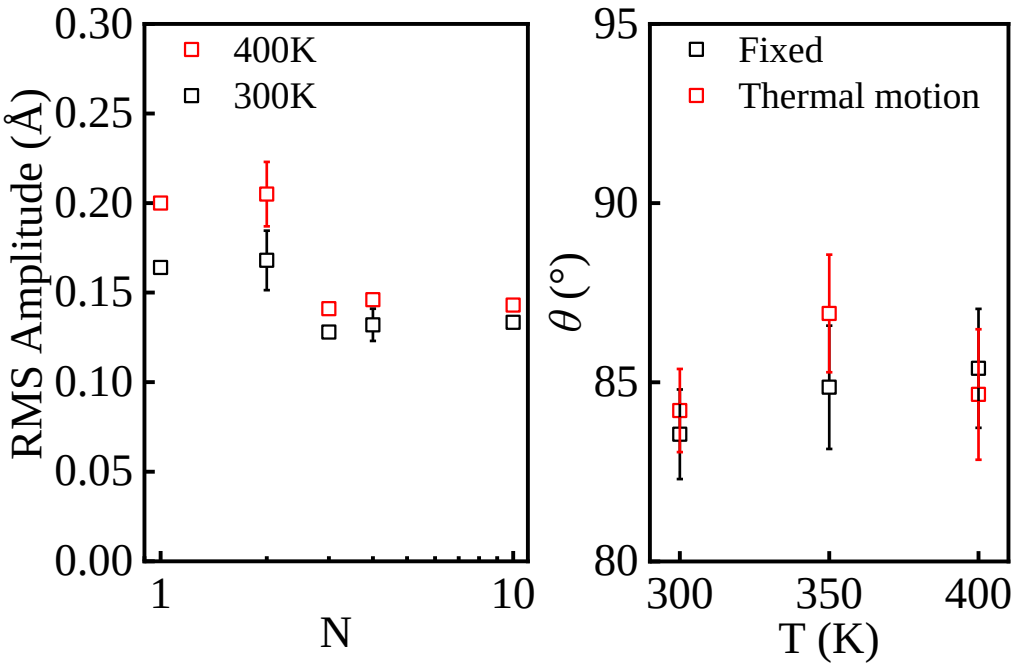

Figure 3. Left: RMS displacement of all substrate carbon atoms in the wall-normal direction as a function of the number N of graphene sheets for two temperatures as indicated. Right: contact angle of water against water vapour on a two-layer graphite substrate as a function of temperature for fixed and thermally excited graphite. On data points without error bars, the uncertainty is less than the symbol size.

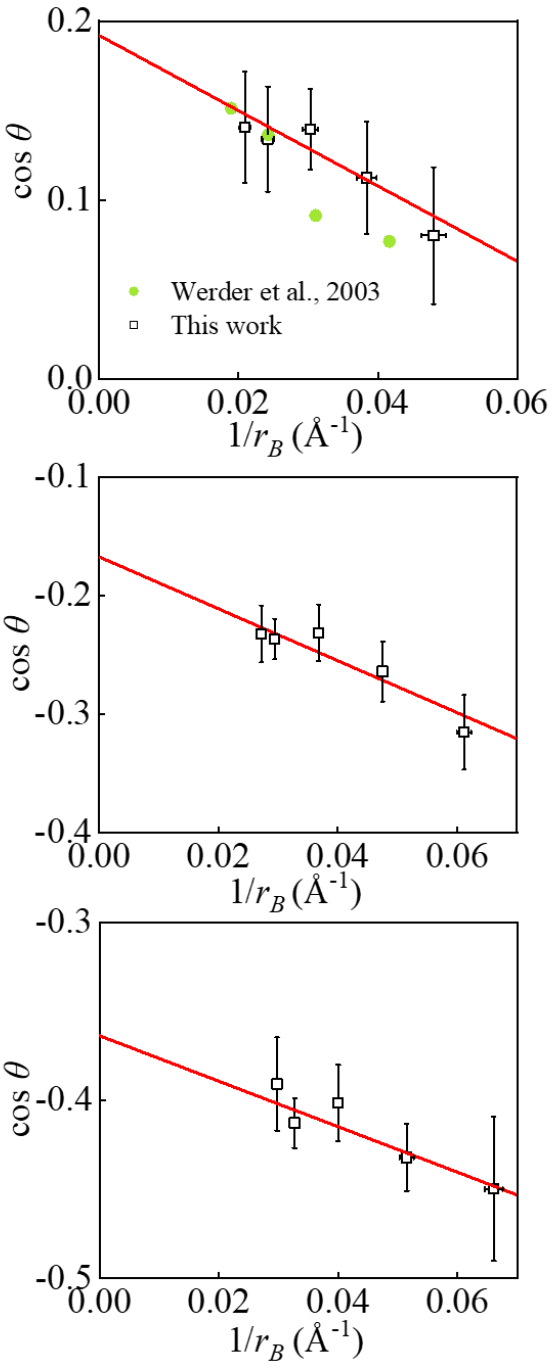

Figure 4. Cosinus of the contact angle versus inverse droplet radius. Top: water only at a pressure of 0.0014 MPa. Middle: water in CH_4 at a pressure of 3.0 MPa. Bottom: water in CO_2 at a pressure of 3.5 MPa. The red line is a least-squares linear fit through our data points. In all cases: T=300 K.

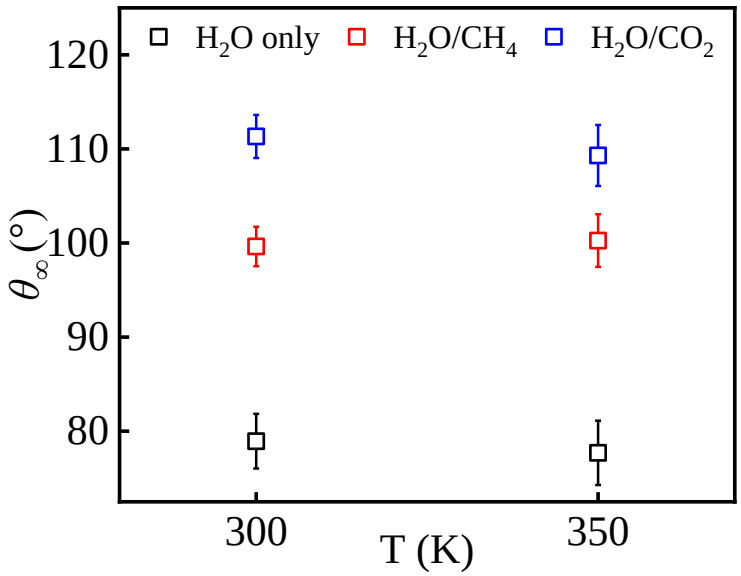

Figure 5. Macroscopic contact angle for H_2O only, H_2O/CH_4 and H_2O/CO_2 systems at T=300K and 350K.

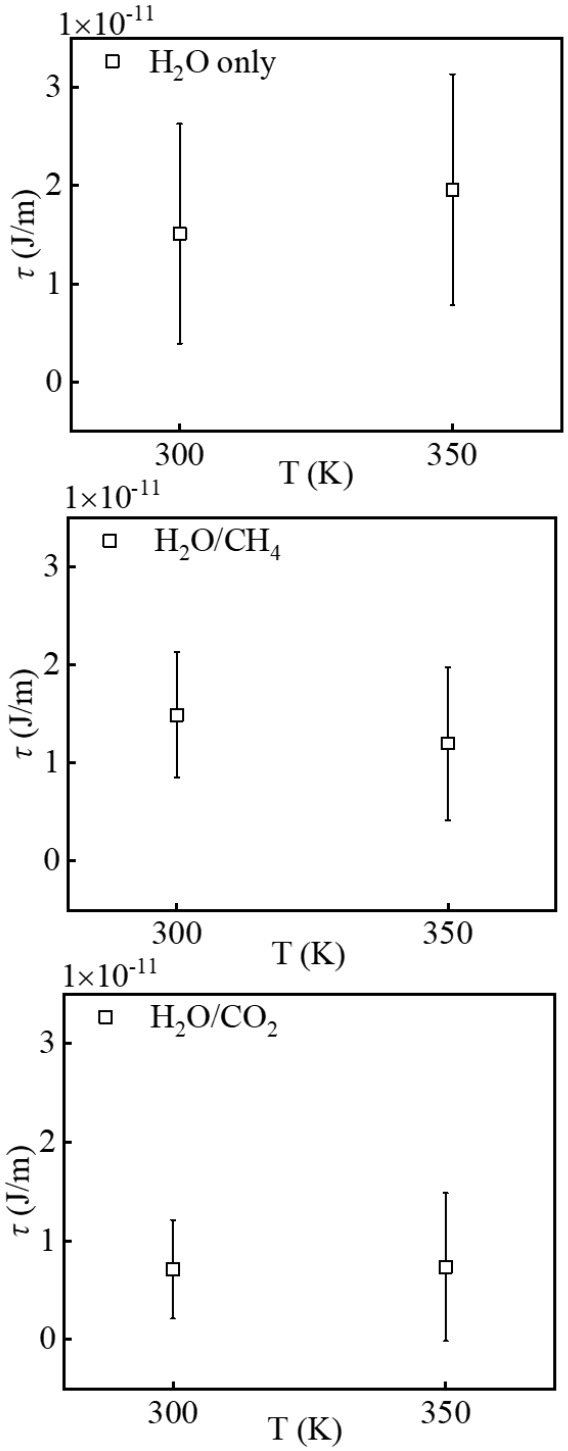

Figure 6. Line tension for H_2O only, H_2O/CH_4 and H_2O/CO_2 systems at T=300K and 350K.

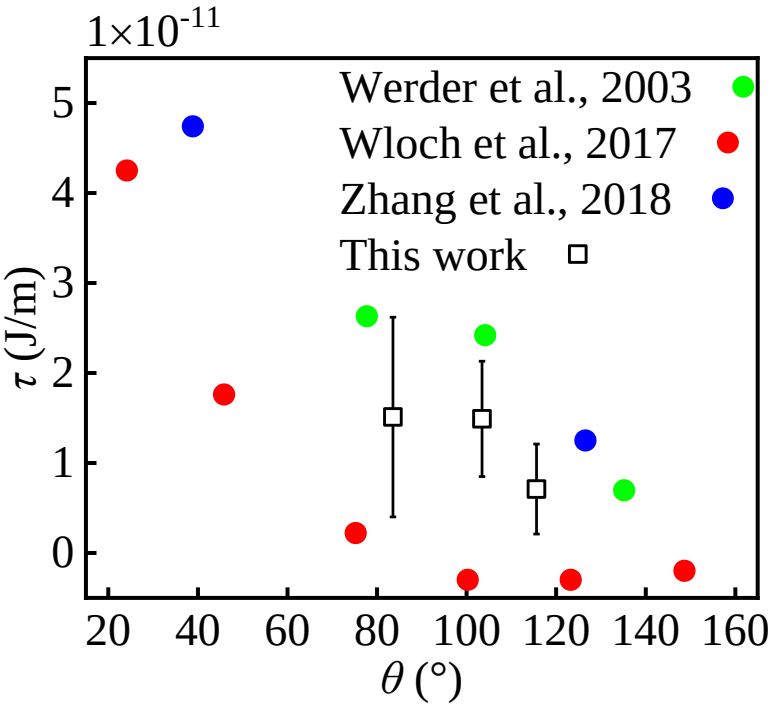

Figure 7. Comparison of the relationship between line tension and water droplets contact angles on a variety of surfaces, at T=300K.

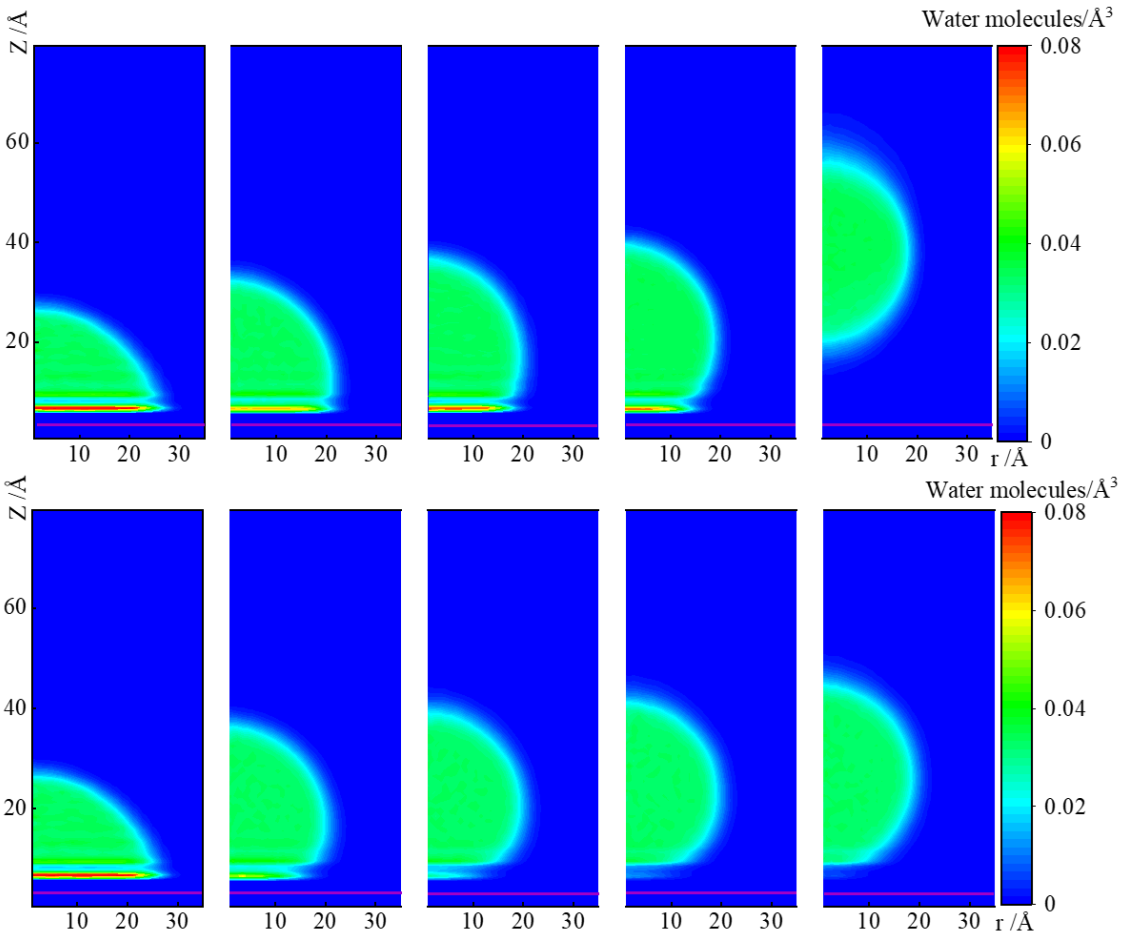

Figure 8. The impact of CH_4 and CO_2 on averaged water molecular concentration at T=300K. Top: CH_4 as continuous phases, from left to right, P (CH_4) equals to 0, 5.56, 11.2, 44.6, 78.7 MPa; bottom: CO_2 as continuous phase, CO_2 molecules equals to 0, 5.14, 8.0, 10.7, 12 MPa. Red horizontal line represents the top graphite surface.

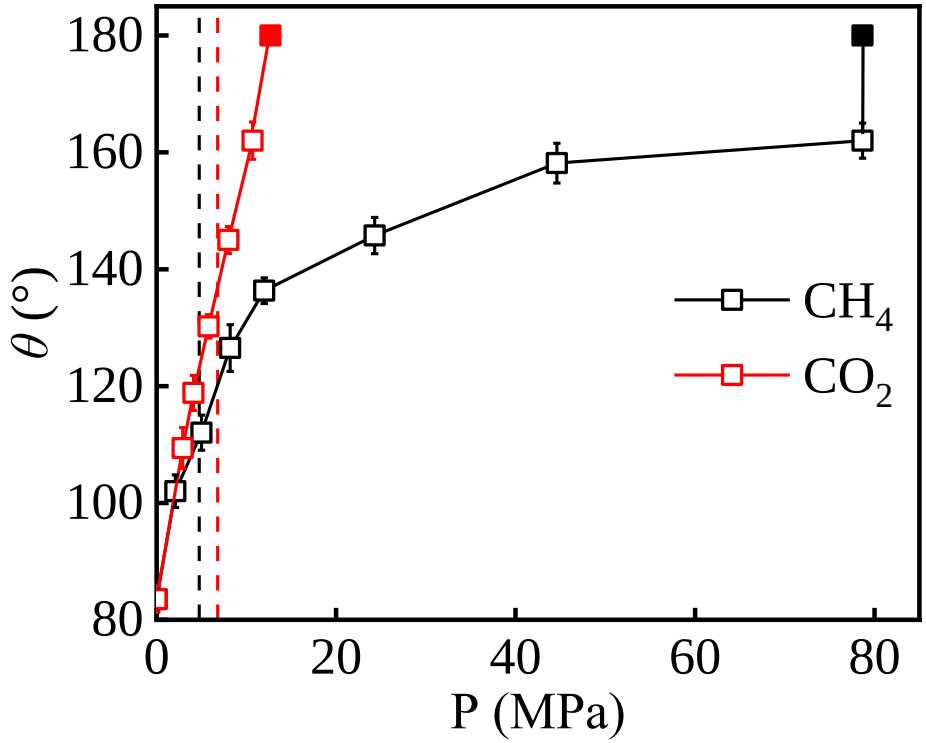

Figure 9. Contact angle of water on graphite in a CH_4 and CO_2 environment as a function of pressure at 300 K. The black vertical dashed line is the critical pressure of CH_4; the red dashed line is the saturation pressure of CO_2. Filled symbols indicate the droplet has detached from the surface.

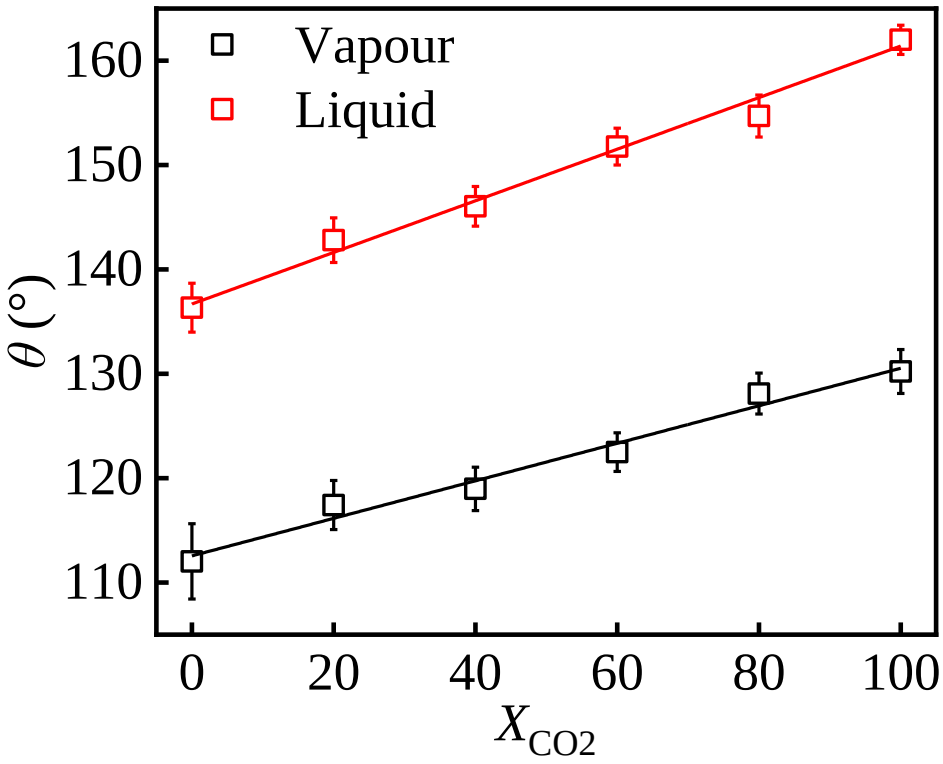

Figure 10. Mole fraction CO_2 versus contact angle of a water droplet on graphite in a CH_4 / CO_2 mixture at 300 K at a pressure of 10.70 MPa (liquid) and 5.36 MPa (vapour). The lines are a linear function that best fit the data points.

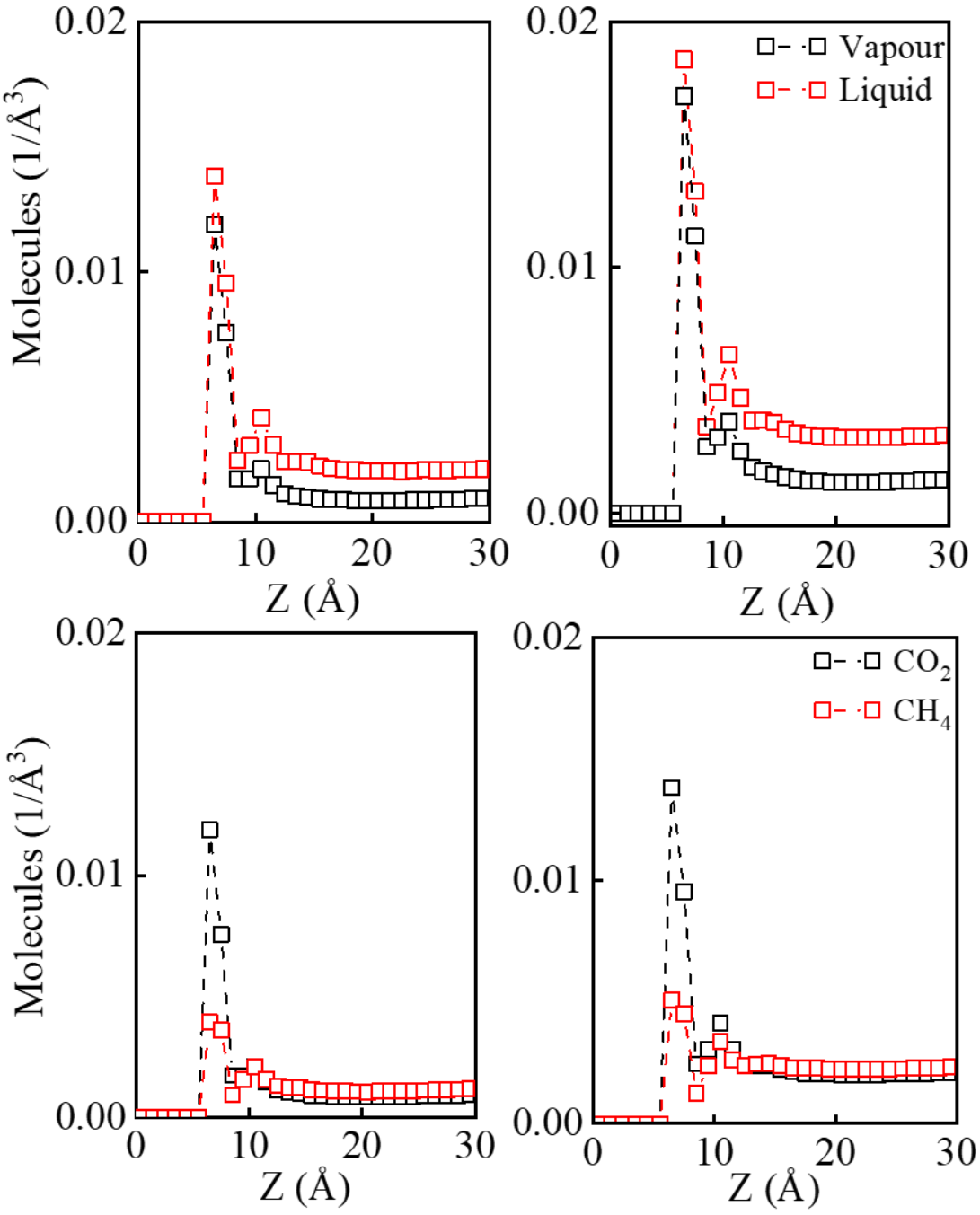

Figure 11. Number density profile perpendicular to the graphite surface (Z direction). Top: vapour and liquid CO_2 density profile at X_{CO2}=40% (left) and X_{CO2}=60% (right). Bottom: comparison with the 40% CO_2 (X_{CO2}=40%) and 40% CH_4 (X_{CO2}=60%) density profile at vapour (left) and liquid (right) condition.